Discrete element modeling of edge-on-impact tests on concrete

Andria Antoniou, Pascal Forquin, Laurent Daudeville

Computational Particle Mechanics manuscript No.
(will be inserted by the editor)

Discrete element modeling of edge-on-impact tests on concrete

Andria Antoniou[1] · **Pascal Forquin**[1] · **Laurent Daudeville**[1*]

Received: date / Accepted: date

Abstract Concrete is widely utilized in the construction of critical structures such as nuclear plants, explosive material storage bunkers, and water-retaining facilities. These concrete constructions must be designed to withstand potential threats from terrorist attacks or accidental events, such as projectile impacts. When a slab undergoes severe impact loading, the concrete material experiences high loading rates and encounters a complex stress state, characterized by high confined compression stress near the point of projectile impact and tensile stresses near the slab's free edges. This can result in potential spalling and scabbing on the front and rear faces of the slab. Addressing this issue, the discrete element method (DEM) proves particularly effective due to its capability to handle discontinuities with ease. To this end, a DEM model was implemented in the industrial computer program Europlexus, a finite element code for analyzing fluid-structure systems under transient dynamic loading. In previous studies, the authors introduced a compaction model accounting for pore closure and free water presence in concrete, validated through simulations of penetration tests on thick concrete targets with passive confinement. This paper shifts focus to the DEM simulation of edge-on impact tests conducted on non-confined concrete tiles using ogive-nose projectiles. Unlike the aforementioned penetration tests, these original experiments involve moderate mean stress, highlighting the influence of tensile stresses on the fracturing process. The results validate the model's ability to accurately represent fracturing and cratering processes in concrete, which are highly dependent on loading rates.

Keywords Discrete element model · Impact · Concrete · Edge-on impact · Strain rate effect

*Corresponding author: Laurent Daudeville
E-mail: laurent.daudeville@univ-grenoble-alpes.fr
[1]Univ. Grenoble Alpes, CNRS, Grenoble INP, 3SR, 38000 Grenoble, France

1 Introduction

The safety and the protection of sensitive infrastructures, such as nuclear power plants, dams, and explosive storage facilities, are of paramount importance. Protection measures against accidental impacts (e.g., vehicle collisions or airplane crashes) and intentional attacks (e.g., missile strikes) require appropriate design methodologies to mitigate potential catastrophic consequences. When a concrete slab is impacted by a rigid projectile, it undergoes various stages of high-intensity stress, resulting in different damage mechanisms depending on projectile velocity and slab thickness. These mechanisms include cratering and spalling on the front face, triaxial compression within the penetration zone where confinement stress arises due to the inertia of the surrounding material, and scabbing on the rear face due to tensile stresses near the free surface [1], [2], [3]. Current design approaches for protective concrete shields used in sensitive infrastructures mainly rely on full-scale experiments and empirical formulas derived from extensive testing and observations [2], [4], [5], [6]. While practical and reliable, these methods often lack a strong theoretical foundation or rigorous numerical validation. Additionally, the high cost of full-scale experiments and the limited applicability of empirical formulas highlight the need for advanced numerical tools.

The Finite Element Method (FEM) is widely used for nonlinear structural analysis. However, when modeling fracturing or fragmentation phenomena in impact

scenarios, FEM typically relies on erosion criteria that lack physical significance and require case-specific calibration [7], [8].

Originally developed by Cundall et al. [9] for modeling granular media, the Discrete Element Method (DEM) has proven effective for simulating advanced damage states, including those in cohesive materials. Its discontinuous nature allows for the explicit representation of macro-cracks and fragmentation, making it particularly suitable for capturing complex failure mechanisms.

Over the years, Daudeville et al. developed a DEM model for concrete under severe loading conditions [10], [11], [12], [13], [14]. This model has been implemented into Europlexus [15], an industrial finite element code developed for analyzing fluid-structure interactions under transient dynamic loading, co-owned by the CEA (French alternative energies and atomic energy commission) and the Joint Research Centre of the European Commission.

Validating an advanced concrete behavior model that accounts for brittle damage, compaction under high confining pressure, and strain rate dependency requires robust experimental data. Experimental studies conducted at 3SR laboratory, University Grenoble Alpes, using the high-capacity triaxial press Giga [16] have investigated key factors of the well-studied R30A7 ordinary concrete under quasi-static loading conditions, including the loading path [17], [18], [19], [20], water-to-cement ratio [21], coarse aggregate shape and composition [22], matrix porosity [23], water saturation ratio [24] and interstitial pore water pressure [25]. Additionally, Erzar et al. [26] performed spalling experiments to assess the high strain rate tensile strength in concrete R30A7.

To analyze concrete damage under severe dynamic loading, missile impact tests were conducted on 800 mm diameter plain concrete targets with thicknesses of 300 mm and 800 mm and confined with steel jackets [7], [27]. The targets were made of the reference ordinary concrete R30A7. These perforation and penetration experiments provided a reference for validating the DEM concrete model implemented in Europlexus. The influence of saturation ratio on penetration was investigated by Benniou et al. [28]. The validation of the model accounting for both dynamic confinement and strain-rate effects was carried out by Antoniou et al. [29]. It is important to note that in penetration experiments, the material near the impact zone experiences high compressive stresses, leading to irreversible compaction. Regions farther from the impact site undergo moderate confined compression (CC) [30], while tensile damage is mainly limited to the free edges. Consequently, such tests are not ideal for validating constitutive models describing concrete fracturing under dynamic loading.

Concrete strength exhibits strain-rate dependency, particularly under tensile loading, as demonstrated by Malvar et al. [31]. They characterized dynamic strength enhancement in tension using the dynamic increase factor (DIF), defined as the ratio of dynamic to static strength. They modeled DIF evolution as a bilinear function of the strain rate, distinguishing between moderate and high rate regimes, with a transition point around 1 s^{-1}. Fracture energy of concrete is also sensitive to loading rates. Schuler et al. [32] observed that fracture energy increases with higher loading rates, while Weerheijm et al. [33] reported that rate-dependent softening curves shift towards increased brittleness at elevated strain rates. In contrast, strain-rate effects in compression are much lower [34]. Cusatis [35] showed that for unconfined compression (UC) tests at strain rates exceeding 10^{-1} s^{-1}, inertial forces contribute significantly to observed strength enhancement. Accurately incorporating strain-rate effects into concrete models is crucial for describing fracturing processes under dynamic loads.

This study aims to validate the DEM model's ability to simulate concrete fracturing at different loading rates. The key innovation of this research lies in both integrating all dissipative nonlinear phenomena into a unified DEM model and simulating original edge-on impact (EOI) tests conducted on non-confined concrete tiles impacted by ogive-nose projectiles. The advantage of EOI tests is that they generate fracturing under low mean stress conditions.

The paper is structured as follows: Section 2 summarizes the DEM model and parameter identification for concrete, as detailed by Antoniou [29]. Section 3 presents the experimental setup for EOI tests. Section 4 compares DEM simulations with experimental results, demonstrating the model's predictive capability.

2 DEM model for concrete

The model was detailed in [29]. It is briefly reminded in this section.

2.1 Constitutive model description

Discrete elements (DE) are rigid spherical elements where mass is concentrated, possessing six degrees of freedom (three translational and three rotational), and initially linked by beam-like cohesive interactions. The characteristic size of DE does not correspond to individual concrete constituents, such as aggregates. Instead, the

Table 1 Mechanical properties of R30A7 concrete [24]

Porosity accessible to water (%)	12
Density (kg.m^{-3})	2280
Slump (cm)	7
Young modulus E (GPa)	25
Poisson ratio ν	0.16
Compressive strength σ_c (MPa)	34
Tensile strength (MPa)	3.6

DEM model operates at a larger scale, aiming to replicate the macroscopic behavior of concrete in both linear and nonlinear regimes. The mechanical properties of ordinary concrete R30A7 studied in this article are provided in Table 1. The maximum aggregate size (8 mm) was chosen in accordance with the dimensions of specimens (70 mm in diameter and 140 mm in length) tested with the Giga high-capacity triaxial press [16].

The behavior of undamaged plain concrete is assumed to be isotropic and homogeneous. To create an assembly of spherical DE with varying diameters, the studied concrete specimen geometry is first meshed with finite element (FE) tetrahedra. A geometrical process developed by Jerier et al. [36] is then applied to generate spheres of different sizes and integrate them into the FE mesh with the maximum compactness. The isotropic nature of the constitutive behavior of the DE assembly can be assessed by ensuring that the distribution of interaction orientations remain uniform in all spatial directions.

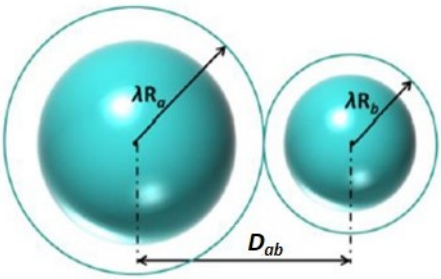

Fig. 1 Cohesive interaction.

A cohesive interaction (Fig. 1) is initially established between two DE, denoted as a and b, with radii R_a and R_b and separated by a distance D_{ab}, if $\lambda(R_a+R_b)>D_{ab}$, where λ is the interaction range coefficient.

For each DE assembly, λ is determined to ensure an average of 12 interactions per DE. That empirical choice ensures the isotropy of the DE assembly [12].

If a cohesive interaction breaks, a new contact interaction may form between the two DEs if they come into direct contact ($\lambda = 1$). Table 2 provides all the interaction parameters.

Table 2 Parameters of interaction between DE a and b [29]

D_{ab} (m)	Distance between DE a and b
R_a, R_b (m)	Radii of DE a and b
S_{int} (m^2)	Interaction surface
λ	Interaction range coefficient
F_N, F_S (N)	Normal and shear forces
K_N, K_S (N/m)	Normal and shear stiffnesses
α, β, γ	Stiffness parameters
K_r (Nm)	Rolling stiffness
β_r	Rolling stiffness parameter
D_{init} (m)	Initial distance between DE
D_{max} (m)	Distance between DE at failure
T (Pa)	Tensile strength
T_{st} (Pa)	Static tensile strength
T_{dyn} (Pa)	Dynamic tensile strength
M_{plas} (Nm)	Yield moment
η	Yield moment parameter
DIF	Dynamic increase factor
DIF_{max}	Maximum dynamic increase factor
ξ	Softening parameter ($DIF = 1$)
ξ_{DIF}	Softening parameter for DIF
ξ_{max}	Softening parameter for DIF_{max}
C_0 (Pa)	Cohesion
C_{cel} (Pa)	Compressive yield stress
C_{cpl} (Pa)	Consolidation stress
ϕ_i	Friction angle of cohesive interaction
ϕ_c	Friction angle of contact interaction
ξ_1	Hardening coefficient
ξ_2	Consolidated material hardening coeff.
$\dot{\epsilon}_{st}$ (s^{-1})	Quasi-static strain rate
$\dot{\epsilon}_m$ (s^{-1})	Moderate strain rate
δ_1	Moderate strain-rate regime slope
δ_2	High strain-rate regime slope

The elastic behavior between DE is characterized by normal stiffness K_N and tangential stiffness K_S, which are linked to the macroscopic elastic properties, Young's modulus E, and Poisson's ratio ν, through micro-macro relations (1), (2), as established by Hentz et al. [37].

$$K_N = \frac{E.S_{int}}{D_{init}} \cdot \frac{1+\alpha}{\beta(1+\nu)+\gamma(1-\alpha\nu)} \tag{1}$$

$$K_S = K_N \frac{1-\alpha\nu}{1+\nu} \tag{2}$$

Where D_{init} is the initial distance between the DE, and S_{int}=πMin(R_a^2, R_b^2) denotes the interaction surface.

A rolling resistance mechanism limits local rotations, thereby influencing the brittle nature of the macroscopic constitutive behavior. To model this, the link between DE a and b is modeled as a cylindrical elastic beam with a radius r = Min(R_a, R_b). The rolling elastic stiffness is K_r (3), the rolling resistance moment is limited to M_{plas} (4) (Fig. 2). T denotes the local tensile

strength (Fig. 3) and the bending inertia is defined as $I=\frac{\pi.r^4}{4}$.

$$K_r = \beta_r \frac{E.I}{D_{ab}} \tag{3}$$

$$M_{plas} = \eta \frac{T.I}{r} \tag{4}$$

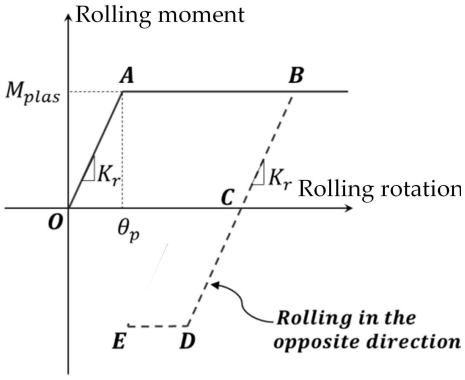

Fig. 2 Moment-rotation behavior.

α, β, and γ in (1) and (2) represent parameters specific to the DE assembly. Potapov et al. [14] demonstrated that the elastic properties of the generated DE assembly remain minimally affected by discretization, provided that the packing technique parameters — such as the ratio of maximum to minimum DE radii, the ratio of the average DE radius to the average FE size, and the random distribution of DE sizes — are kept constant.

The non-linear constitutive behavior in tension compression is depicted on Fig. 3 (compressive forces are considered positive). The tensile behavior is initially elastic with damage progression. Softening behavior, governed by the coefficient ξ, begins when the normal force F_N reaches $S_{int}T$. The interaction is considered broken once the distance D_{ab} exceeds D_{max}.

Shear behavior and tensile strength follow a classical modified Mohr-Coulomb criterion, defined by a tension cut-off T, cohesion C_0, and the friction angles ϕ_i and ϕ_c for the cohesive and contact interactions, respectively.

Under compression, the constitutive behavior is elastic plastic with bilinear hardening, to describe compaction under high mean stress (right side of Fig. 3). Once the yield strength $S_{int}.C_{cel}$ is exceeded, porosity closure induces hardening. Complete consolidation of the material is achieved when the compressive force surpasses $S_{int}.C_{cpl}$. The two hardening regimes are characterized by coefficients ξ_1 and ξ_2.

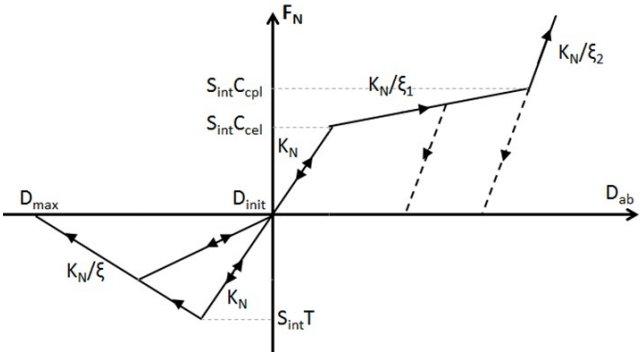

Fig. 3 Constitutive model for the normal interaction.

Vu et al. [24] demonstrated the significant influence of free water content on the response of concrete under triaxial compression at high confinement. Benniou et al. [28] slightly modified the present model by incorporating the local parameter S_r, the water saturation ratio assigned to each DE. When S_r reaches unity, the fully consolidated material accounts for the additional contribution of water stiffness and the maximum shear stress is capped. The influence of free water content on the compressive response of unconfined or moderately confined concrete is much less pronounced than under high levels of confinement, whether in quasi-static or dynamic conditions. Therefore, the influence of free water is not considered in the present study.

2.2 Strain rate effect

This subsection examines the effect of loading rate, which is crucial for accurately describing fracturing. Proper consideration of this effect is essential to ensure the fidelity of the model.

The rate dependency of concrete in tension is significant [31] and is primarily attributed to its heterogeneous microstructure [33], [38]. To maintain accuracy, the presented macro-model must incorporate this effect.

Experimental results from Split-Hopkinson Pressure Bar (SHPB) tests indicate a slight increase in apparent compressive strength with increasing strain rate [34]. However, studies by Cusatis et al. [35] and Ruiyuan et al. [39] suggest that this enhancement in SHPB experiments is primarily due to radial inertial forces. Consequently, strain-rate sensitivity at the macro-scale is significantly more pronounced in tension than in compression.

Thus, in the present DEM model, the loading rate effect at the DE scale is considered only in tension. Hentz et al. [10] demonstrated that incorporating strain-rate effects in tension at the DE scale enables accurate

reproduction of SHPB compression experiments at the macro-scale.

The DIF evolution is given in (5)-(6), where σ_c represents the concrete compressive strength, and σ_{c0} (set at 10 MPa) serves as a reference value.

$$DIF = \frac{T_{dyn}}{T_{st}} = \begin{cases} 1 & \text{if } \dot{\epsilon} \leq \dot{\epsilon}_{st} \\ (\frac{\dot{\epsilon}}{\dot{\epsilon}_{st}})^{\delta_1} & \text{if } \dot{\epsilon}_{st} \leq \dot{\epsilon} \leq \dot{\epsilon}_m \\ \theta(\frac{\dot{\epsilon}}{\dot{\epsilon}_{st}})^{\delta_2} & \text{if } \dot{\epsilon}_m \leq \dot{\epsilon} \end{cases} \quad (5)$$

$$\text{where } \delta_1 = \frac{1}{1+8\frac{\sigma_c}{\sigma_0}} \text{ and } \theta = (\frac{\dot{\epsilon}_m}{\dot{\epsilon}_{st}})^{(\delta_1-\delta_2)} \quad (6)$$

Erzar et al. [40] demonstrated that the shear response of concrete exhibits strain-rate dependency, though to a significantly lesser extent than in tension. The corresponding DIF in shear is capped at a maximum value of 2.0. By applying the modified Mohr-Coulomb criterion, the maximum DIF in tension is determined using (7).

$$DIF_{max} = \frac{2.0 \times C_0}{T_{st} \times tan\phi_i} \quad (7)$$

In addition to the increase in tensile strength, Weerheijm et al. [33] observed a slight increase in fracture energy, accompanied by a steeper post-peak slope as the strain rate increases. Similarly, Schuler et al. [32] determined that the dynamic fracture energy at higher strain rates is approximately 2 to 3 times greater than its static counterpart. Building on these observations, Fig. 4 illustrates the proposed modeling of tensile constitutive behavior, which incorporates increases in both tensile strength and fracture energy.

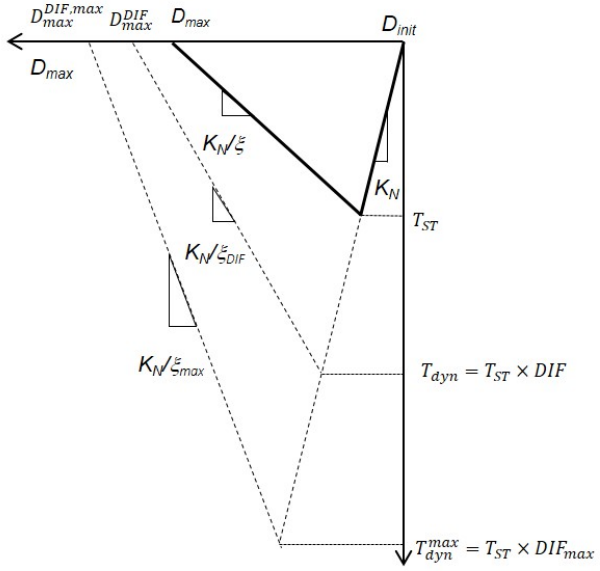

Fig. 4 Influence of loading rate on tensile constitutive behavior

2.3 Identification of DEM model parameters for R30A7 concrete

The identification of contitutive behavior parameters in Table 2 is based on simulations of quasi-static (QS) and dynamic laboratory tests conducted on specimens made of R30A7 concrete. These simulations were presented by Antoniou et al. [29].

- Parameters influencing the macroscopic elastic behavior are calibrated by means of a few linear simulations of QS UC tests [37]. Identified values: $\alpha = 3.9, \beta = 3.75$, and $\gamma = 5$.
- Parameters influencing the macroscopic nonlinear constitutive behavion under QS tension and compression (strength and post-pic behavior) are identified through UC test simulations. Identified values: β_r =5, η =5, T_{st} =2.5 MPa, $\xi = 3$, $C_0 = 4.5$ MPa, ϕ_i =20°, and ϕ_c=20°.
- Parameters influencing the constitutive behavior under high mean stress are identified through simulations of CC tests performed with the high capacity triaxial press Giga. Identified values: $\xi_1 = 1.5, \xi_2 = 0.3, C_{cel} = 50$ MPa, and $C_{cpl} = 300$ MPa.
  It is worth noting that these parameters have a minimal effect on the simulation of EOI tests presented in the next section, as concrete tiles remain unconfined.
- Parameters influencing the strain-rate dependency are identified thanks to data taken from [31], [32], thanks to Eq. (7), and through simulations of SHPB tensile tests. Identified values: $DIF_{max} = 10, \xi_{max} = 2.56, \dot{\epsilon}_{st} = 10^{-6}s^{-1}, \dot{\epsilon}_m = 1\ s^{-1}, \delta_1 = 0.0355, \delta_2 = 0.333$.

3 Edge-on impact tests

The EOI test was initially developed by Kalthoff et al. [41] to investigate the fragmentation of brittle materials, such as glass, under high strain rates. This experiment is particularly well-suited for analyzing dynamic fragmentation, as the thin material tile remains unconfined. Consequently, this test is highly relevant for validating the DEM damage model at high strain rates and low mean stress. Another advantage of the test is its ability to provide visualization of damage evolution, effectively simulating loading conditions equivalent to a ballistic impact in a two-dimensional configuration.

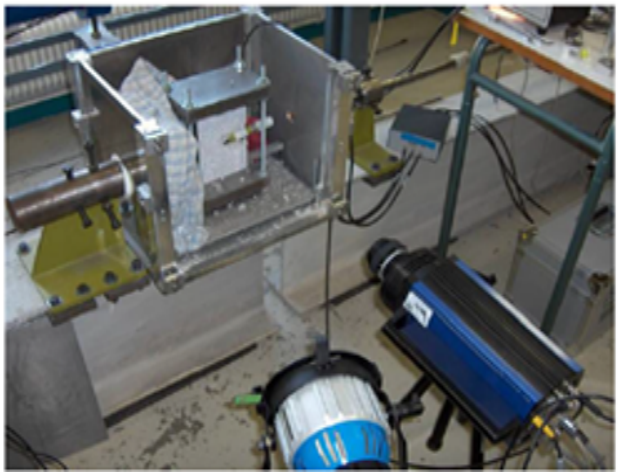

Fig. 5 Edge-on impact setup

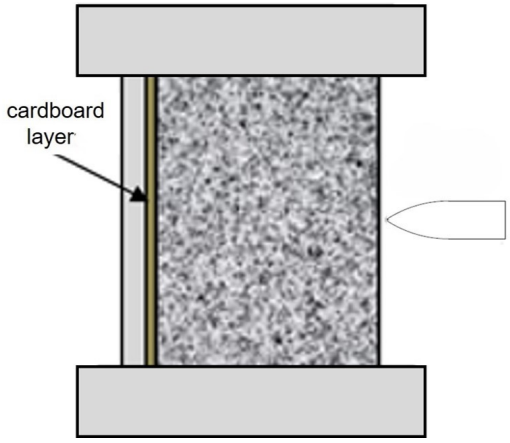

Fig. 6 Concrete tile target and projectile

Erzar et al. [42] performed EOI tests on plain concrete R30A7 using the following setups (Fig. 5 and Fig. 6): a cylindrical ogive-nose steel projectile impacts a thin concrete tile with dimensions 20 x 12 x 1.5 cm^3. To ensure controlled boundary conditions, two rigid steel plates constrain the vertical displacements of the top and bottom specimen faces, while a flexible vertical steel plate and a cardboard layer limit the horizontal displacement of the tile's rear face.

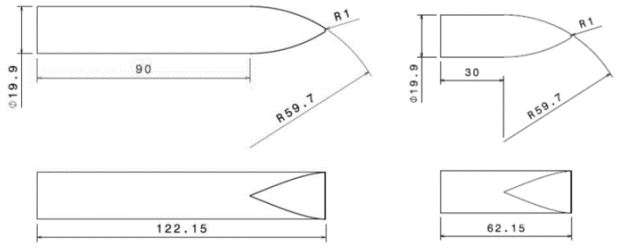

Fig. 7 Geometries of the two projectiles

Two EOI tests were conducted using 1.99cm diameter projectiles, categorized as follows:

- Short projectile: 62.15 mm in length, 130.4 g in mass, launched at 76 ms^{-1}.
- Long projectile: 122.15 mm in length, 273.9 g in mass, launched at 56 ms^{-1}.

Fig. 7 shows the geometries of the two projectiles.

4 Simulation of the two edge-on impact tests

The concrete tile is modeled using DE, while tetrahedral FE and hexahedral FE are employed for the projectiles and three steel plates, respectively. Two of these plates constrain the vertical displacements of the top and bottom specimen faces, whereas a flexible vertical plate with fixed ends limits the horizontal displacement of the tile's rear face (the cardboard layer is not included in the model). A linear elastic behavior is assumed for the steel projectile and supports with Young's modulus $E_{steel} = 210$ GPa and Poisson's ratio $\nu_{steel} = 0.3$.

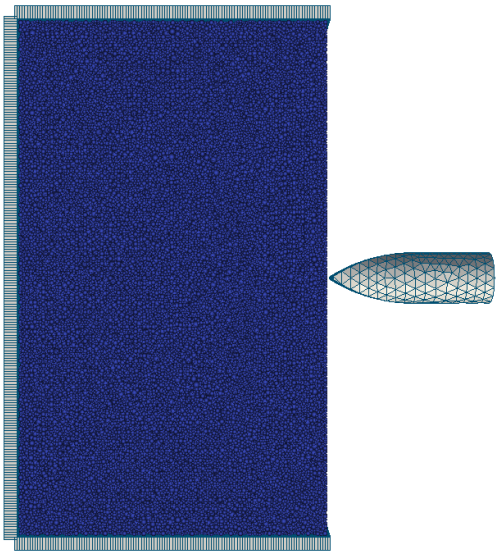

Fig. 8 DE/FE model of EOI test with the short projectile launched at 76 ms^{-1}

The concrete DE assembly is composed of 118,209 DE with a maximum radius of 1.4 mm, a minimum radius of 0.47 mm, and a compactness of 0.61. Fig. 8 illustrates the EOI test model with the FE short projectile and the DE concrete tile enclosed by the three FE plates. All parameters of the concrete DEM model

were determined prior to the simulations, based on laboratory test simulations performed on R30A7 concrete, as detailed in section 2.3.

Fig. 9 Final damage state of the tile tested with the short projectile launched at 76 ms^{-1}

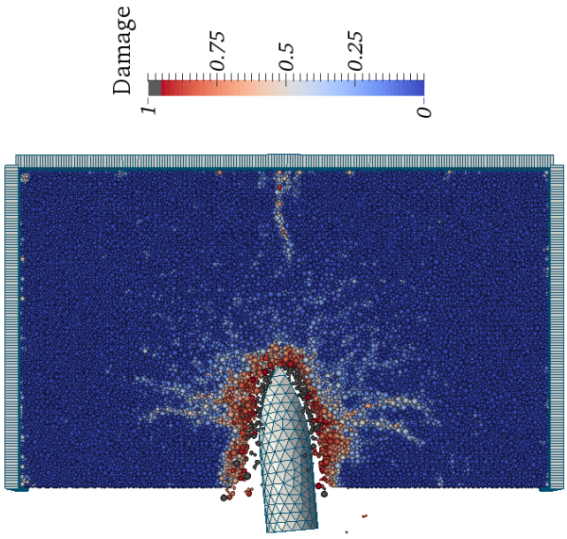

Fig. 10 Calculated final damage state of the tile tested with the short projectile launched at 76 ms^{-1}

Fig. 9 shows the final damage stage of the tile tested with the small projectile. Fig. 10 presents the results from the numerical simulation. The number of broken links of a DE divided by its total number of initial links defines the damage indicator for the considered DE. The damage pattern is in good agreement with the experiment. Note that the projectile trajectory is not aligned with the symmetry axis of the target because of the random distribution of DE.

Fig. 11 displays the time evolution of the projectile penetration in the target, the calculated penetration depth of the projectile corresponds well to the experimental one.

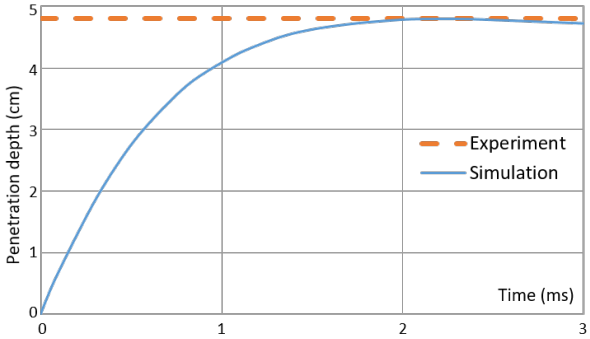

Fig. 11 Calculated penetration depth of the short projectile launched at 76 ms^{-1}

Similarly, Fig. 12 shows the final damage stage of the tile tested with the long projectile. Fig. 13 presents results from the numerical simulation that are in good agreement with the experiment, especially for the cratering damage. The calculated penetration depth of the projectile corresponds to the experimental one as can be seen in Fig. 14.

Fig. 12 Final damage state of the tile tested with the long projectile launched at 56 ms^{-1}

The results of these two EOI test simulations validate the capability of the DEM concrete model to accurately describe dynamic fracturing. This phenomenon is primarily driven by tensile stresses, which are highly dependent on the loading rate.

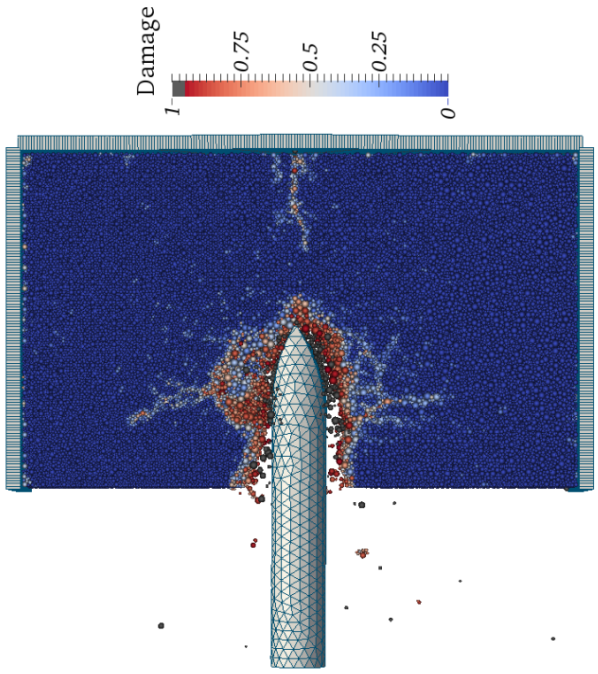

Fig. 13 Calculated final damage state of the tile tested with the long projectile launched at 56 ms^{-1}

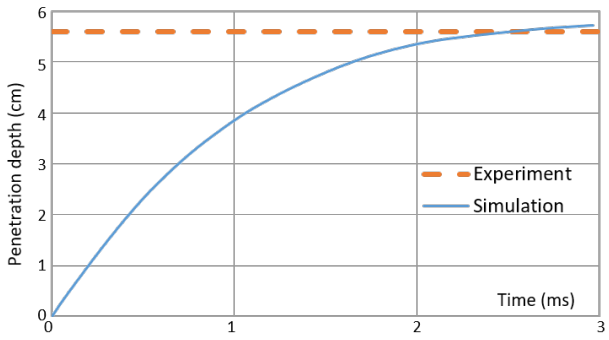

Fig. 14 Calculated penetration depth of the long projectile launched at 56 ms^{-1}

5 Conclusion

This article presents a DEM concrete model implemented in Europlexus for simulating concrete structures under impulsive loading. The model accounts for key non-linear dissipative phenomena occurring during severe dynamic events, including: brittle damage in tension, which is highly dependent on loading rate, compaction in triaxial compression under high confinement, and transition from brittle to ductile behavior under triaxial compression with moderate confinement.

The DE interaction laws were identified in previous studies [10], [12], [14], [29], [37], utilizing simulations of laboratory tests, including quasi-static confined compression tests [17], [24] and Split-Hopkinson Pressure Bar (SHPB) tensile and compressive tests [40].

The DEM model's capability to describe concrete damage in thick targets subjected to projectile penetration has been demonstrated by Antoniou [29]. While tensile stresses may occur near free edges, the results of these tests are primarily governed by compaction and shear phenomena under high mean stress.

The correct description of fracturing process under impact loading is crucial and challenging because of its coupling with other dissipative phenomena. Accurately describing the fracturing process under impact loading is crucial and challenging due to its coupling with other dissipative phenomena. To assess the DEM model's ability to simulate concrete fracture under dynamic loading, the edge-on impact test is selected. This test minimizes triaxial confinement stresses in the concrete tile, thereby emphasizing the influence of tensile stresses in the fracturing process.

Two edge-on impact tests performed on ordinary concrete are simulated and compared with experimental results. These tests, involving two different impact conditions, allow for the investigation of loading rate effects. The simulations accurately predict the penetration depth of each projectile and replicate the observed damage patterns, which consist of a cratering zone and several main cracks.

In conclusion, this study, along with previous works, demonstrates that the DEM model for concrete implemented in Europlexus is a predictive tool capable of determining both the depth of projectile penetration into concrete and the resulting damage in the impacted zone. This capability is crucial for a variety of defensive and non-defensive applications.

Acknowledgements This research was financially supported by EDF company.

Conflict of interest

The authors declare that they have no conflict of interest.

Data availability

The authors declare that the data supporting the findings of this study are available within the paper and in its references.

References

1. Zukas J (1992) Penetration and perforation of solids. Krieger Publishing Co.
2. Li Q, Reid S, Wen H, Telford A (2005) Local impact effects of hard missiles on concrete targets. International Journal of Impact Engineering 32(1-4):224–284.
3. Chen X, Fan S, Li Q (2008) Oblique and normal perforation of concrete targets by a rigid projectile. International Journal of Impact Engineering 30:617–637.
4. Kennedy R P (1976) A review of procedures for the analysis and design of concrete structures to resist missile impact effects. Nuclear Engineering and Design 37(2):183-203.
5. Adeli H, Amin A M (1985) Local effects of impactors on concrete structures. Nuclear Engineering and Design 88(3):301–317.
6. Berriaud C, Sokolovsky A, Gueraud R, Dulac J, Labrot R (1978) Comportement local des enceintes en beton sous l'impact d'un projectile rigide: Local behaviour of reinforced concrete walls under missile impact. Nuclear Engineering and Design 45(2): 457-469.
7. Bian H, Jia Y, Pontiroli C, Shao JF (2018) Numerical modeling of the elastoplastic damage behavior of dry and saturated concrete targets subjected to rigid projectile penetration. International Journal of Numerical and Analytical Methods in Geomechics. 42: 312– 338.
8. Kristoffersen M, Toreskås O.L, Dey S, Børvik T (2021) Ballistic perforation resistance of thin concrete slabs impacted by ogive-nose steel projectiles. International Journal of Impact Engineering, 156, 103957.
9. Cundall P.A., Strack O.D. (1979) A discrete numerical model for granular assemblies. Geotechnique, 29(1), 47-65.
10. Hentz S, Donze FV, Daudeville L (2004) Discrete element modelling of concrete submitted to dynamic loading at high strain rates. Computers and Structures. 82 (29-30): 2509-2524.
11. Frangin E, Marin P, Daudeville L (2006) On the use of combined finite/discrete element method for impacted concrete structures. Journal de Physique IV, 134: 461-466.
12. Rousseau J, Frangin E, Marin P, Daudeville L (2008) Damage prediction in the vicinity of an impact on a concrete structure: a combined FEM/DEM approach. Computers and Concrete, 5(4): 343-358.
13. Shiu W, Donze FV, Daudeville L (2009) Influence of the reinforcement on penetration and perforation of concrete targets. Engineering Computations, 26: 29-45.
14. Potapov S, Mazurel A, Marin P, Daudeville L (2017) Mixed DEM/FEM modeling of advanced damage in reinforced concrete structures. Journal of Engineering Mechanics, 143(2): 04016110.
15. Europlexus, A computer program for analysis of fast transient phenomena involving structures and fluids in interaction, http://www-epx.cea.fr. Accessed 3 Feb 2025.
16. Gabet T, Vu X. H, Malecot Y, Daudeville L (2006) A new experimental technique for the analysis of concrete under high triaxial loading. Journal de Physique IV, 134: 635-640
17. Gabet T, Malecot Y, Daudeville L (2008) Triaxial behavior of concrete under high stresses: Influence of the loading path on compaction and limit states. Cement and Concrete Research, 38(3):403–412.
18. Vu XH, Malecot Y, Daudeville L (2009) Strain measurements on porous concrete samples for triaxial compression and extension tests under very high confinement. The Journal of Strain Analysis for Engineering Design, 44(8):633-657.
19. Dupray F, Malecot Y, Daudeville L (2010) Experimental behaviour of high-performance concrete in confined tension. Materials and structures, 43, 699-707.
20. Malecot Y, Daudeville L, Dupray F, Poinard C, Buzaud E (2010). Strength and damage of concrete under high triaxial loading. European Journal of Environmental and Civil Engineering, 14(6-7): 777-803.
21. Vu XH, Malecot Y, Daudeville L, Buzaud E (2009) Effect of the water/cement ratio on concrete behavior under extreme loading. International Journal for Numerical and Analytical Methods in Geomechanics, 33:1867-1888
22. Poinard C, Piotrowska E, Malecot Y, Daudeville L, Landis E (2012) Compression triaxial behavior of concrete: the role of the meso-structure by analysis of x-ray tomographic images. European Journal of Environmental and Civil Engineering, 16(S1):115–136.
23. Malecot Y, Zingg L, Briffaut M, Baroth J (2019) Influence of free water on concrete triaxial behavior: The effect of porosity. Cement and Concrete Research, 120: 207-216.
24. Vu XH, Malecot Y, Daudeville L, Buzaud E (2009) Experimental analysis of concrete behavior under high confinement: effect of the saturation ratio. International Journal of Solids and Structures, 46:1105–1120.
25. Accary A, Malecot Y, Daudeville L (2019) Design and evaluation of a deformable sensor for interstitial pore pressure measurement in concrete under very high stress level. Applied Sciences, 9(13):2610.
26. Erzar B, Forquin P (2010) An experimental method to determine the tensile strength of concrete at high rates of strain. Experimental Mechanics, 50(7):941–955.
27. Pontiroli C, Erzar B, Buzaud E (2014) Concrete behavior under ballistic impacts: Effects of materials parameters to penetration resistance and modeling with PRM model. Computational Modelling of Concrete Structures, 2:685–693.
28. Benniou, H, Accary A, Malecot Y, et al (2021) Discrete element modeling of concrete under high stress level: influence of saturation ratio. Comp. Part. Mech. 8, 157–167.
29. Antoniou A, Daudeville L, Marin P, Potapov S (2024) Extending the discrete element method to account for dynamic confinement and strain-rate effects for simulating hard impacts on concrete targets. Journal of Dynamic Behavior of Materials, 1-17.
30. Gran JK, Frew DJ (1979) In-target radial stress measurements from penetration experiments into concrete by ogive-nose steel projects. International Journal of Impact Engineering, 19: 715–726.
31. Malvar L, Ross C (1998) Review of strain rate effects for concrete in tension. Materials Journal, 95(6):735–739.
32. Schuler H, Mayrhofer C, Thoma K (2006) Spall experiments for the measurement of the tensile strength and fracture energy of concrete at high strain rates. International Journal of Impact Engineering, 32(10):1635–1650.
33. Weerheijm J, Forquin P (2013) Response mechanisms of concrete under impulsive tensile loading. In: Understanding the Tensile Properties of Concrete, 181-217, Woodhead Publishing
34. Bischoff PH, Perry SH (1991) Compressive behavior of concrete at high strain rates. Materials and Structures, 24(6):425–450.
35. Cusatis G (2011) Strain-rate effects on concrete behavior. International Journal of Impact Engineering, 38(4): 162-170.
36. Jerier JF, Imbault D, Donzé FV, Doremus P (2009) A geometric algorithm based on tetrahedral meshes to generate a dense polydisperse sphere packing. Granular Matter 11(1): 43-52.
37. Hentz S, Daudeville L, Donze FV (2004). Identification and validation of a discrete element model for concrete. Journal of engineering mechanics, 130(6): 709-719.

38. Gatuingt F, Snozzi L, Molinari JF (2013) Numerical determination of the tensile response and the dissipated fracture energy of concrete: role of the mesostructure and influence of the loading rate. International Journal for Numerical Analytical Methods in Geomechanics 37(18): 3112-3130.
39. Ruiyuan H, Zhenhuang G, Jian Q, Yanbo W, Zhichao L (2024) Strain rate effect of concrete based on split Hopkinson pressure bar (SHPB) test. Journal of Building Engineering 86, 108856.
40. Erzar B, Forquin P (2014) Analysis and modeling of the cohesion strength of concrete at high strain-rates. International Journal of Solids and Structures, 51(14), 2559-2574.
41. Kalthoff JF, Senf H, Winkler S, Hornemann U, Rothenhaüsler H, Experimental investigation of wave and fracture propagation in glass slabs loaded by steel cylinders at high impact velocities, Conference on the Mechanical Properties of Materials at High Rates of Strain 1984. Proceedings, 291-298, Institute of Physics - Conference Series, 70, Oxford (1984)
42. Erzar B, Forquin P (2011). Experiments and mesoscopic modelling of dynamic testing of concrete, Mechanics of Materials, 43(9): 505-527.